

See discussions, stats, and author profiles for this publication at: <https://www.researchgate.net/publication/26832405>

# Dynamic Properties of a Psychrophilic $\alpha$ -Amylase in Comparison with a Mesophilic Homologue

ARTICLE in THE JOURNAL OF PHYSICAL CHEMISTRY B · SEPTEMBER 2009

Impact Factor: 3.3 · DOI: 10.1021/jp900790n · Source: PubMed

---

CITATIONS

15

READS

18

## 5 AUTHORS, INCLUDING:



Marco Pasi

École Polytechnique Fédérale de Lausanne

12 PUBLICATIONS 199 CITATIONS

[SEE PROFILE](#)



Laura Riccardi

Istituto Italiano di Tecnologia

9 PUBLICATIONS 131 CITATIONS

[SEE PROFILE](#)



Luca De Gioia

Università degli Studi di Milano-Bicocca

213 PUBLICATIONS 5,335 CITATIONS

[SEE PROFILE](#)



Elena Papaleo

Danish Cancer Society

66 PUBLICATIONS 629 CITATIONS

[SEE PROFILE](#)

# Dynamic Properties of a Psychrophilic $\alpha$ -Amylase in Comparison with a Mesophilic Homologue

Marco Pasi, Laura Riccardi, Piercarlo Fantucci, Luca De Gioia, and Elena Papaleo\*

Department of Biotechnology and Biosciences, University of Milano-Bicocca, P.zza della Scienza 2, 20126 Milan, Italy

Received: January 27, 2009; Revised Manuscript Received: July 18, 2009

The cold-active, chloride-dependent  $\alpha$ -amylase from *Pseudoalteromonas haloplanktis* (AHA) is one of the best characterized psychrophilic enzymes, and shares high sequence and structural similarity with its mesophilic porcine counterpart (PPA). An atomic detail comparative analysis was carried out by performing more than 60 ns of multiple-replica explicit-solvent molecular dynamics simulations on the two enzymes in order to characterize the differences in ensemble properties and dynamics in solution between the two homologues. We find in both enzymes high flexibility clusters in the surroundings of the substrate-binding groove, primarily involving the long loops that protrude from the main domain's barrel structure. These loops are longer in PPA and extend further away from the core of the barrel, where the active site is located: essential fluctuations in PPA mainly affect the highly solvent-accessible portions of these loops, whereas AHA is characterized by greater flexibility in the immediate surroundings of the active site. Furthermore, detailed analysis of active-site dynamics has revealed that elements previously identified through X-ray crystallography as involved in substrate binding in both enzymes undergo concerted motions that may be linked to catalysis.

## Introduction

In recent years, there has been increased interest in the origin of enzyme adaptation to low temperatures both for understanding protein folding and structure–function relationship<sup>1–4</sup> and for biotechnological and industrial applications.<sup>5,6</sup> The number of reports on enzymes from cold-adapted organisms has increased significantly over the past years, and reveals that adaptive strategies are variable among enzymes,<sup>3,4,7,8</sup> and involve the adjustment of different structural features. In particular, the current view suggests that in cold environments, during evolution, the strong selective pressure for cold activity,<sup>8,9</sup> and the lack of selective pressure for thermostable proteins,<sup>10</sup> resulted in highly active enzymes characterized by distinct structural flexibility at temperatures that tend to freeze molecular motions.<sup>3,9,11</sup>

Molecular flexibility at low temperatures has been generally assumed to be related to a decrease in the number or weakening of intramolecular interactions in comparison to the mesophilic counterparts.<sup>3,4,8,11</sup> Cold-adapted enzymes generally differ from their mesophilic or thermophilic homologues only for subtle structural characteristics and/or few amino acid substitutions. In fact, it has been shown that amino acidic substitutions in crucial functional regions, as well as greater hydrophilicity of solvent exposed surfaces, can enhance the overall or local structural flexibility.<sup>3,4,8,12,13</sup>

The cold-active, chloride-dependent  $\alpha$ -amylase from the Antarctic bacterium *Pseudoalteromonas haloplanktis* (AHA) is one of the best characterized psychrophilic enzymes. Its biochemical properties and X-ray structure have been extensively studied in the context of enzyme catalysis at low temperature.<sup>14–27</sup> In particular, AHA was one of the first cold-adapted enzymes for which the X-ray structure was solved,<sup>16,17</sup> revealing that the enzyme consists of three domains (Figure 1).

Domain A is at the N-terminus and is composed of a  $(\beta/\alpha)_8$ -barrel forming one side of the catalytic cleft, domain B protrudes from domain A and forms the other side of the active cleft, and domain C is the C-terminal domain. A  $\text{Ca}^{2+}$  ion is bound between domains A and B, and a  $\text{Cl}^-$  ion which is necessary for catalysis is bound close to the active site. The enzyme is a glycosyl-hydrolase and features two acid catalytic residues: the proton donor (E200) and the catalytic nucleophile (D174); a second conserved aspartic acid residue (D264) possibly has the role of stabilizing the protonated state of the glutamic side chain.<sup>28</sup>

The X-ray structure of AHA is similar to that of  $\alpha$ -amylases from mammalian species, such as porcine  $\alpha$ -amylase (PPA), which is inherently more thermally stable than AHA,<sup>18,22</sup> a characteristic common to mesophilic enzymes. Comprehensive structural and biochemical studies of these two enzymes have highlighted that AHA features lower core hydrophobicity and looser packing of hydrophobic residues,<sup>16</sup> and low conformational stability of the active-site region, possibly linked with localized increases in conformational flexibility.<sup>25</sup>

In the present study, we carried out a computational investigation based on molecular dynamics (MD) simulations, in order to better elucidate structural and molecular features of the cold-adapted  $\alpha$ -amylase in comparison with its mesophilic homologue. MD is a suitable tool to evaluate flexibility and correlate flexibility with protein structure and function.<sup>29–34</sup> In addition, MD simulations can be used to rationalize experimental results, allowing the interpolation or extrapolation of empirical data into regions hardly accessible otherwise.<sup>32,33,35</sup> In fact, long and multiple MD simulations aimed at clarifying structure–function relationship in cold-adapted enzymes have recently been reported for serine proteases<sup>29,36,37</sup> and for uracil–DNA glycosylases.<sup>38,39</sup>

A study of the overall flexibility of AHA has been recently presented in the context of 1 ns MD simulations of several psychrophilic enzymes.<sup>40</sup> However, the authors concluded that

\* To whom correspondence should be addressed. E-mail: elena.papaleo@unimib.it.

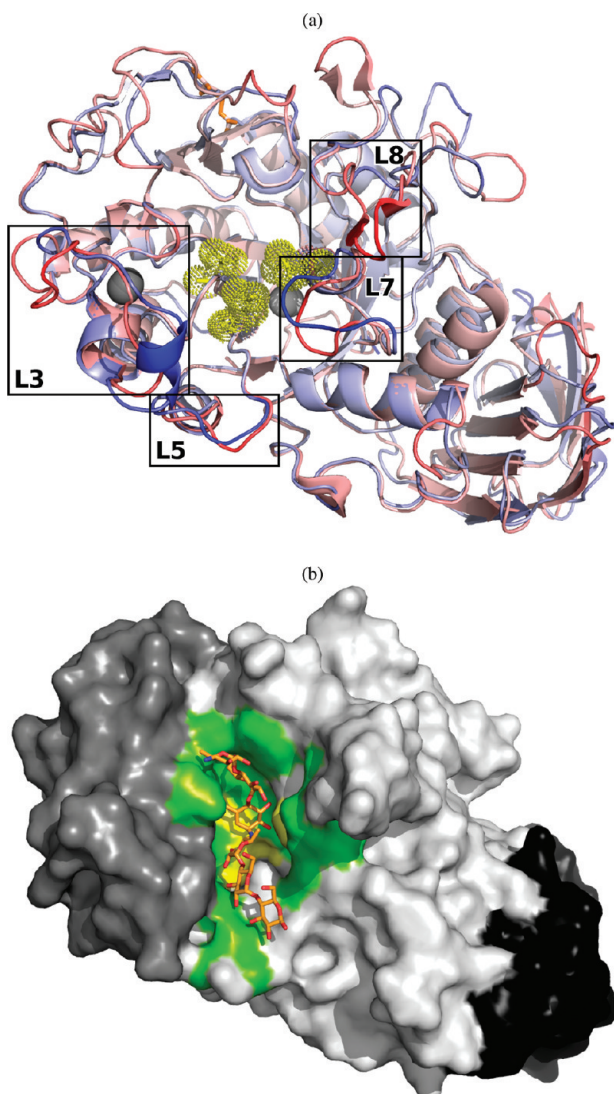


**Figure 1.** (a) Cartoon representation of the crystal structures of PPA and AHA, superimposed and colored in shades of red and blue, respectively, with color intensity proportional to flexibility; (b) surface representation of PPA, showing a substrate (from crystal structure 1PIG after superposition of the two proteins); the substrate-binding groove is colored green, while the three domains are colored white (domain A), gray (domain B), and black (domain C). The chloride (white) and calcium (gray) ions are shown as spheres, the C70–C115<sup>P</sup> disulfide bridge, missing in AHA, is shown as orange sticks, and the catalytic triad is shown as yellow dots and sticks.

longer trajectories are necessary in order to provide a better statistical insight and elucidation of structural flexibility of selected enzymes. In fact, it is well-known that the analysis of long multiple trajectories helps in the identification of recurring features and can allow avoidance of artifacts arising from the simulation procedure.<sup>41,42</sup> Given the importance of the simulation time scale and conformational sampling,<sup>33,41</sup> several MD simulations of the psychrophilic and mesophilic enzymes were carried out in explicit solvent at room temperature (298 K), allowing the collection of 36 ns MD trajectories for each system. These trajectories have been analyzed in terms of secondary structure content, solvent accessibility, intramolecular interactions, and molecular flexibility, revealing a striking degree of similarity of the dynamical properties of the two enzymes; comparison of flexibility of the active-site region allows us to suggest possible adaptive traits and to identify concerted motions in the active site of the two enzymes which may be linked to catalysis.

## Methods

**Molecular Dynamics Simulations.** MD simulations, and some analyses, were performed using a modified version<sup>43,44</sup> of the GROMOS-87<sup>45</sup> united-atom force-field with the GROMACS software version 3.2 ([www.gromacs.org](http://www.gromacs.org)). The X-ray structures of native porcine (PPA) and *Pseudoalteromonas haloplanktis* (AHA)  $\alpha$ -amylase (PDB entries 1PIF<sup>46</sup> and 1AQH,<sup>16</sup> respectively) were used as the starting point for the simulations. After a careful visual inspection of the structures, minor corrections were made in order to obtain a perfect match with the primary sequence of the enzymes, available as SwissProt entries P00690 and P29957, respectively. In particular, in 1AQH, the missing side chain of E118 was restored by *in-silico* mutagenesis with PyMOL ([www.pymol.org](http://www.pymol.org)), while in 1PIF the N-terminal pyroglutamic acid, which is due to a physiological post-translational modification,<sup>47</sup> was replaced with a proline residue, which is structurally very similar and has the advantage of being more suitable to being treated by the force-field.

To improve conformational sampling, six independent simulations (*replicas*) were carried out at constant temperature and pressure (298 K and 1 bar) in explicit solvent, for each protein system, initializing the MD runs with different sets of initial atomic velocities taken from a Maxwellian distribution. Periodic boundary conditions were used with a box size of 534.8 and 539.0 nm<sup>2</sup>, containing 15090 and 15224 SPC<sup>48</sup> water molecules for AHA and PPA, respectively. The LINCS<sup>49</sup> algorithm was used to constrain covalent bonds in the protein, and long-range electrostatic interactions were evaluated using PME.<sup>50</sup> The time step used was 2 fs, and sampled conformations were stored every 2 ps. Full details on the preparation and simulation procedures are available as Supporting Information text S1; details on other analyses are available as Supporting Information text S2.

**Stability of MD Trajectories.** The root-mean-square deviation (rmsd), which is a crucial parameter to evaluate the stability of MD trajectories, was computed for main-chain atoms with respect to the starting structure of the simulations, and its time evolution (see Supporting Information Figure S1) was monitored along with other relevant structural properties, such as the protein radius of gyration and the distance between the calcium and chloride ions and their coordinating residues.

All *replicas* have been conducted for 6 ns, except trajectories showing the slowest convergence times (above 2.5 ns, *replicas* 2, 5, and 6 of AHA), which have been elongated to 11 ns. For each protein, the equilibrated portions of the six *replicas* were joined to obtain a concatenated metatrajectory, which is representative of different directions of sampling around the starting structures. PPA trajectories were considered to have established equilibrium between 0.2 and 2.0 ns, whereas AHA trajectories generally required longer equilibration times (0.9 ns up to 4.0 ns). After concatenating the equilibrium portions of the trajectories, the resulting analysis ensembles consisted of 36.50 and 29.74 ns for the psychrophilic and mesophilic  $\alpha$ -amylases, respectively.

**Molecular and Structural Properties.** The secondary structure content was calculated for all stored conformations using the DSSP program, which defines secondary structural elements based on hydrogen-bonding patterns and geometrical features.<sup>51</sup> Comparison of the secondary structure patterns of the two enzymes was performed using the ensemble averages divided by the number of amino acids considered, for the whole enzyme as well as for single protein domains (Table 1).

To take into account the dynamic properties of secondary structures, their time evolution was analyzed in detail by evaluating the most frequently attained secondary structure for

**TABLE 1:** Ensemble Average of the Secondary Structure Content in AHA and PPA, According to the DSSP Software<sup>52 a</sup>

		PPA			AHA		
	secondary str	$\langle x \rangle$	$\pm \sigma$	[%]	$\langle x \rangle$	$\pm \sigma$	[%]
total	$\beta$ -strand	103.090	$\pm 9.115$	[20.784%]	94.622	$\pm 7.783$	[21.121%]
	$\beta$ -bridge	15.529	$\pm 3.699$	[3.131%]	15.550	$\pm 3.514$	[3.471%]
	$\alpha$ -helix	100.097	$\pm 4.248$	[20.181%]	106.616	$\pm 4.734$	[23.798%]
	bend	75.198	$\pm 6.724$	[15.161%]	73.368	$\pm 5.897$	[16.377%]
	turn	66.671	$\pm 6.870$	[13.442%]	47.823	$\pm 6.499$	[10.675%]
	coil	118.534	$\pm 6.277$	[23.898%]	96.919	$\pm 5.675$	[21.634%]
	$\beta$ -strand	50.815	$\pm 6.396$	[15.260%]	39.267	$\pm 4.434$	[13.266%]
domain A	$\beta$ -bridge	5.245	$\pm 2.830$	[1.575%]	5.662	$\pm 2.243$	[1.913%]
	$\alpha$ -helix	95.137	$\pm 3.802$	[28.570%]	98.451	$\pm 4.505$	[33.260%]
	bend	39.115	$\pm 5.360$	[11.746%]	48.701	$\pm 4.389$	[16.453%]
	turn	43.801	$\pm 5.800$	[13.153%]	28.040	$\pm 5.686$	[9.473%]
	coil	84.637	$\pm 4.452$	[25.417%]	66.354	$\pm 3.650$	[22.417%]
	$\beta$ -strand	3.870	$\pm 2.479$	[5.451%]	7.958	$\pm 3.217$	[13.263%]
	$\beta$ -bridge	6.395	$\pm 1.853$	[9.007%]	6.147	$\pm 2.287$	[10.245%]
domain B	$\alpha$ -helix	4.960	$\pm 1.808$	[6.986%]	8.163	$\pm 2.849$	[13.605%]
	bend	19.706	$\pm 2.681$	[27.755%]	10.801	$\pm 2.685$	[18.002%]
	turn	12.702	$\pm 2.999$	[17.890%]	6.334	$\pm 2.809$	[10.557%]
	coil	22.843	$\pm 2.338$	[32.173%]	18.342	$\pm 2.691$	[30.570%]
	$\beta$ -strand	48.282	$\pm 5.679$	[52.480%]	46.676	$\pm 5.743$	[50.735%]
	$\beta$ -bridge	1.267	$\pm 0.979$	[1.377%]	1.778	$\pm 1.504$	[1.933%]
	$\alpha$ -helix	0.000	$\pm 0.000$	[0.000%]	0.002	$\pm 0.084$	[0.002%]
domain C	bend	15.488	$\pm 3.457$	[16.835%]	10.988	$\pm 2.841$	[11.943%]
	turn	8.181	$\pm 2.224$	[8.892%]	11.941	$\pm 2.650$	[12.979%]
	coil	17.675	$\pm 3.653$	[19.212%]	20.292	$\pm 3.844$	[22.057%]

<sup>a</sup> The mean values ( $\langle x \rangle$ ) and standard deviations ( $\sigma$ ) are shown along with the ratio between  $\langle x \rangle$  and the total number of residues considered (%).

each residue in order to obtain a residue-dependent persistence degree of secondary structure profile (PDSSP). In order to better identify the differences in secondary structure persistence between the mesophilic and psychrophilic  $\alpha$ -amylases, the PDSSPs were mapped on the 3D structures using a color code.

Intramolecular hydrogen bonds (H-bonds) were evaluated using both a donor–acceptor distance cutoff ( $r_{DA} \leq 0.35$  nm) and acceptor–donor–hydrogen angular cutoff ( $\alpha_{ADH} \leq 30^\circ$ ); ensemble averages were normalized using the total number of donors and acceptors.

Surrounding hydrophobicity ( $H_p$ ) was computed for each residue as

$$H_p(i) = \sum_{j \neq i}^N H(r_d - r_{ij}) h_j$$

where the summation runs over the whole protein,  $r_{ij}$  is the distance between the  $C_\alpha$  atoms of residues  $i$  and  $j$ ,  $H(x)$  is the Heaviside step function [ $H(x) = 1$  if  $x \geq 0$ , and zero otherwise],  $r_d$  is the distance cutoff, and  $h_j$  is the hydrophobicity index<sup>52</sup> of residue  $j$  in kcal mol<sup>-1</sup>. Residue profiles were obtained as ensemble averages. The distance cutoff was set to 0.8, previously identified (see ref 53 and references therein) as sufficient to characterize the hydrophobic behavior and both local and nonlocal interactions of amino acids, and has been used in several other studies.

Relative solvent accessible surface (SAS) was calculated for each stored conformation using the NACCESS program.<sup>54</sup>

**Comparison between Simulations.** Residue-based comparison of the two proteins was carried out by matching residues according to a structural alignment between the crystal structures of the two enzymes performed with the DALI algorithm,<sup>55</sup> and then integrated with available structural and functional data (Supporting Information Figure S2). In particular, the correct matching of the catalytic triad, the residues binding the ionic

cofactors and those contributing to disulfide bridges were taken into account.

Amino acid numbers in the text are labeled with a superscript A or P, referring to the sequence of AHA or PPA, respectively. Domains A, B, and C of AHA are composed of residues 1–86/147–356<sup>A</sup>, 87–146<sup>A</sup>, and 357–448<sup>A</sup>, respectively, whereas domains A, B, and C of PPA are composed of residues 1–98/170–404<sup>P</sup>, 99–169<sup>P</sup>, and 405–496<sup>P</sup>.

The visual analysis of protein structures was carried out using PyMOL (<http://www.pymol.org>).

**Flexibility and Dynamics.** The root-mean-square fluctuation (rmsf) per residue was calculated on  $C_\alpha$  atoms, after projection of the trajectories on the *essential subspace* (see on). The rmsf profiles were calculated on the whole concatenated trajectories (*long-time* rmsf profiles) or as the average of nonoverlapping time windows of 100 ps (*short-time* rmsf profiles). The flexibility of matching residues was compared by computing the Pearson correlation coefficient ( $r$ ) and the slope of the linear regression line ( $m$ ) considering only matching residues in the alignment (excluding gaps).

Correlation plots were obtained by first computing correlation matrices<sup>56</sup>  $\hat{C}_{i,j}$  for  $C_\alpha$  atoms, using averaging windows of 1 ns. Correlations were then plotted on the three-dimensional structures by connecting atoms  $i$  and  $j$  with lines, of which the thickness is proportional to  $\hat{C}_{i,j}$ . Since no negative values of  $\hat{C}_{i,j}$  were found in the analyses, only the most significant ( $\hat{C}_{i,j} > 0.4$ ) long-range ( $|i - j| > 12$ ) positive correlations are shown.

Backbone dihedral rotational freedom was evaluated by measuring the interquartile range between the 95th and 5th percentiles of the ensemble distribution of  $\phi$  and  $\psi$  values for each considered residue, after normalizing the angles to fit in the 0–360° range. This procedure was chosen in order to both obtain a significant estimation of the greater part of the statistical dispersion (90% of the sample is taken into account) and disregard outliers.

**Essential Dynamics Analysis.** The essential dynamics (ED) analysis reveals high-amplitude concerted motions in the simulated trajectories, based on the calculation of the eigenvectors of the covariance matrix of the atomic positional fluctuations. The covariance matrix ( $C_{i,j}$ ) was calculated for protein C<sub>α</sub> atom and considering the equilibrated portion of the trajectories: this has been shown to give a correct picture of the essential subspace.<sup>57</sup> ED analysis was performed for all C<sub>α</sub> atoms, and for C<sub>α</sub> atoms of regions 259–282<sup>A</sup> and 295–319<sup>P</sup>.

ED analysis provided further information on conformational sampling. The number of eigenvectors required to obtain the description of 70% of the motion is 12 and 15 for AHA and PPA, respectively; the corresponding subspace is termed *essential subspace*, and is sufficient to describe protein motions at a reasonable level of accuracy.<sup>57</sup> Motions described by the *essential subspace* have been mapped on average 3D structures by representing with ellipsoids (at probability 0.1) the computed anisotropic temperature factors obtained from the per-residue, C<sub>α</sub> anisotropic U-tensors of cross-correlations of motion along the first 12 and 15 eigenvectors for AHA and PPA, respectively. The average 3D structure is defined as the sampled conformation with the least distance (computed as main-chain rmsd) from the algebraic ensemble average of atomic positions.

Convergence of the dynamical properties of the simulated enzymes between *replicas* is a fundamental issue when performing ED analysis. This issue has been addressed by plotting the projections of *replicas* on the first three eigenvectors of the ED analysis on the concatenated metatrajectory (see Supporting Information Figure S3), by measuring the per-*replica* rmsf in the *essential subspace* (see Supporting Information Figure S7) and by computing the similarity between the subspaces described by the first 10 eigenvectors (*rmsip*) obtained performing ED analysis on portions of the metatrajectory of different lengths, generated by combining different sets of *replicas*<sup>58</sup> (Supporting Information Text S2 and Figure S5). Single *replicas* span different, partially overlapping regions of the conformational space, indicating good sampling of the essential subspace (see Supporting Information Figure S3), and display similar fluctuation intensities (see Supporting Information Figure S7) that correlate well with the picture obtained from the full metatrajectory (Figure 4). Nevertheless, at least 20–25 ns and 15–20 ns for AHA and PPA, respectively (i.e., the combination of three to four *replicas*), are needed to reach a reasonable degree of convergence of the directions of principal motions (see Supporting Information Figure S5). Details on other analyses are available as Supporting Information text S2.

## Results and Discussion

**Overall Structural Properties.** Secondary structure plays a central role in the determination of protein architecture and function; therefore, only minor changes are expected to be tolerated in the secondary structure of homologous proteins which are adapted to different temperature ranges.<sup>3,4</sup> Visual inspection of the 3D crystallographic structures clearly shows that the psychrophilic enzyme features shorter β-α loops and a less structured (β,α)-barrel, lacking especially the inner β-structures.<sup>3</sup> Analysis of the 3D representation of PDSSP (Figure 2, see Methods) shows that, during the simulations, in the catalytic domain, the mesophilic enzyme features a greater average percentage of residues participating in the β-strands composing the core of the catalytic domain, the inner barrel, and greater random coil content ascribable to the longer, poorly structured β-α loops. The differences in these loop sizes may also account for the fact that AHA shows a higher α-helix

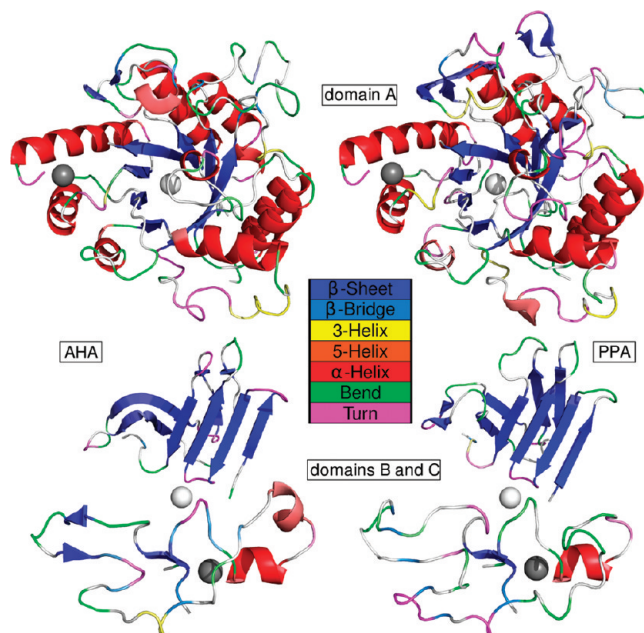


**Figure 2.** 3D representation of the secondary structure persistence in AHA (left) and PPA (right). The secondary structural classes of DSSP definition are adopted and are represented with the color code indicated in the picture. Secondary structure persistence is shown for domain A (top) and domains B and C (bottom), separately.

content, while in PPA the likelihood of turns increases, indicating that the longer loops are not completely unstructured but fail to form real α-helices (Table 1, Figure 2). Domain B of the mesophilic enzyme confirms this last observation, with a greater turn content, and appears to be less orderly structured than in the psychrophilic enzyme; the opposite holds for domain C, which shows a higher content of β-strand in the mesophilic enzyme.

Modulation of the number and type of intramolecular interactions may have provided to cold-adapted enzymes a simple but effective mean to achieve greater structural flexibility, which might be important in order to maintain high catalytic efficiency at low temperatures.<sup>4,59</sup> Hydrogen bonds (H-bonds) are among the strongest nonbonded interactions, and the inverse proportionality of their energy to temperature makes them an interesting issue in cold adaptation. The clustering of hydrophobic side chains within the protein core is another major driving force in the stability of the folded conformation. Comparison of these weak intramolecular interactions between the two α-amylases has been carried out by computing the number of H-bonds, and the number of residues featuring different ranges of  $H_p$  values (the residues surrounding hydrophobicity computed using experimental information, see Methods) for each of the three domains and for domain interfaces, both on crystal structures and on the merged MD trajectories (see Figure 3). Our analyses show a slight decrease in the overall and per-domain number of H-bonds in the mesophilic α-amylases (Figure 3, first set), especially in domains A and C, while greater divergence can be identified in the extension and stability of hydrophobic clusters. AHA shows a greater number of residues with low surrounding hydrophobicity ( $H_p < 10$  kcal mol<sup>-1</sup>, Figure 3, second set), when compared with the mesophilic enzyme, while PPA reveals a rise in the percentage of residues in highly hydrophobic environments ( $H_p > 15$  kcal mol<sup>-1</sup>, Figure 3, third and fourth sets), especially in domain A. These findings correlate with the observed higher stability of

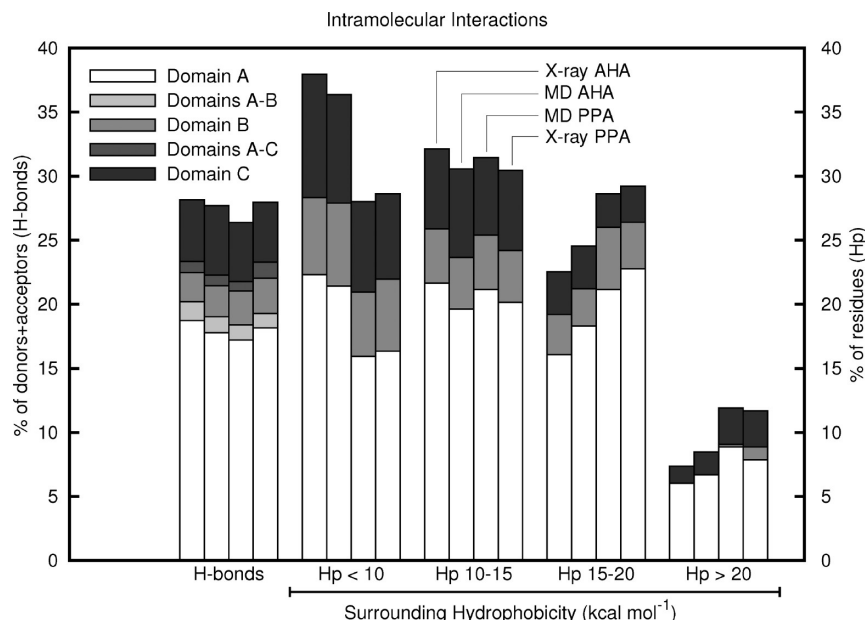


**Figure 3.** Hydrogen bonds and surrounding hydrophobicity ( $H_p$ ) are described as histograms representing the percentage of donors + acceptors involved in H-bonds (first set, y axis on the left) or of residues with surrounding hydrophobicity in the indicated range ( $H_p$ , all other sets, y axis on the right); each set shows values computed for the crystal structure of AHA (1AQH, first), the MD simulations of AHA (second) and PPA (third), and the crystal structure of PPA (1PIF, fourth).

the barrel's core  $\beta$ -strands, and suggest the weakening of core hydrophobicity as a possible adaptive trait.

**Analysis of Structural Flexibility.** Low stability and high catalytic efficiency of cold-adapted enzymes at low temperatures have been related to a flexible protein structure.<sup>9,11,24</sup> Enhanced flexibility is generally found either scattered throughout the entire protein edifice or localized in particular regions.<sup>3,4,13</sup>

In order to evaluate and compare the flexibility in mesophilic and psychrophilic  $\alpha$ -amylases, the root-mean-square fluctuation of  $C_\alpha$  atoms (rmsf) with respect to the ensemble average structure was adopted as the flexibility index. The validity of this flexibility index is supported by the comparison with crystallographic B-factor profiles and computed main-chain amide generalized order parameters<sup>60</sup> ( $S^2$ , see Supporting Information Figure S6).

Secondary structure elements generally exhibit low flexibility in both proteins (Figure 4): peaks in the profiles are located in correspondence of poorly structured loop regions, and although differing remarkably in intensity, they often overlap when the two profiles are aligned. Analysis of profiles taking into account the position of secondary structure elements suggests that not only the latter are conserved in the two proteins but also their degree of flexibility is maintained, especially if the structural elements composing the  $(\beta/\alpha)_8$  barrel are considered.

The wider conformational sampling available allows us to extend the description made of these  $\alpha$ -amylase flexibilities by Spiwok et al.<sup>40</sup> A picture, similar to that previously described, results from using 100 ps windows (Figures 4b and Figure 2a from ref 40); this is remarkable given the differences in the simulation procedure and starting structures, especially for PPA. Although there are slight differences in the alignment used for the comparison, regions featuring low flexibility are generally very similar, while greater divergence can be found in some peak values. When *long-time* fluctuations are considered (Figure 4a), along with a scattered increase in flexibility in the regions featuring low *short-time* rmsf and generally stable secondary structures, significant enhancements can be seen for most peaks. Detailed comparison of *long-time* fluctuations between the two

enzymes allows the identification of four regions featuring significantly higher flexibility in AHA, and three regions fluctuating more in PPA (Table 2). It is interesting to note that many of the highest peaks of the mesophilic enzyme flexibility profile correspond to insertions, i.e., gaps in the aligned sequence of AHA (Table 2).

Structural localization of the regions listed in Table 2 shows that differences in *long-time* flexibility between the two  $\alpha$ -amylases strikingly cluster around the active site and in the substrate-binding groove. For this reason, and to address the analysis toward the marked differences in the catalytic behavior of the two enzymes, the next sections present a detailed description of the character of these two enzymes' active-site flexibility and dynamics.

**Overall Flexibility of the Active Site.** The eight loops that protrude from the  $(\beta/\alpha)_8$  barrel structure above the active site undergo particularly intense motions in our simulations, and represent the most flexible regions surrounding the catalytic triad. Among these, those featuring the most pronounced fluctuations are the portions of loops  $\beta_3-\alpha_3$ ,  $\beta_5-\alpha_5$ , and  $\beta_7-\alpha_7$  that project toward the catalytic triad, forming a three-sided cleft on one side of the substrate-binding groove (**L3**, **L5**, and **L7**, respectively; see Figure 1 and Table 2 for the definition of the abbreviations). Furthermore, all three have been found to be in contact with cocrystallized substrate analogues, and a possible role in the catalytic cycle of both  $\alpha$ -amylases has been suggested for the rearrangement of  $\beta_7-\alpha_7$  in the process of binding and release of the substrate.<sup>47,61-65</sup>

**L3** features low structural similarity between the two enzymes and the greatest fluctuational mobility inside domain B: in AHA, the C-terminal region of **L3** (**L3<sub>C</sub>**) is longer and carries a stable, short, and highly mobile  $\alpha$ -helix, while, in PPA, it is preceded by a highly flexible coil region (the N-terminal region of **L3**, **L3<sub>N</sub>**), which has no correspondence in the structure of the psychrophilic enzyme. The comparison of the intensity and localization of **L3** motions shows that in AHA high flexibility is localized nearer to the catalytic triad than in PPA (see Figure 4a, c).

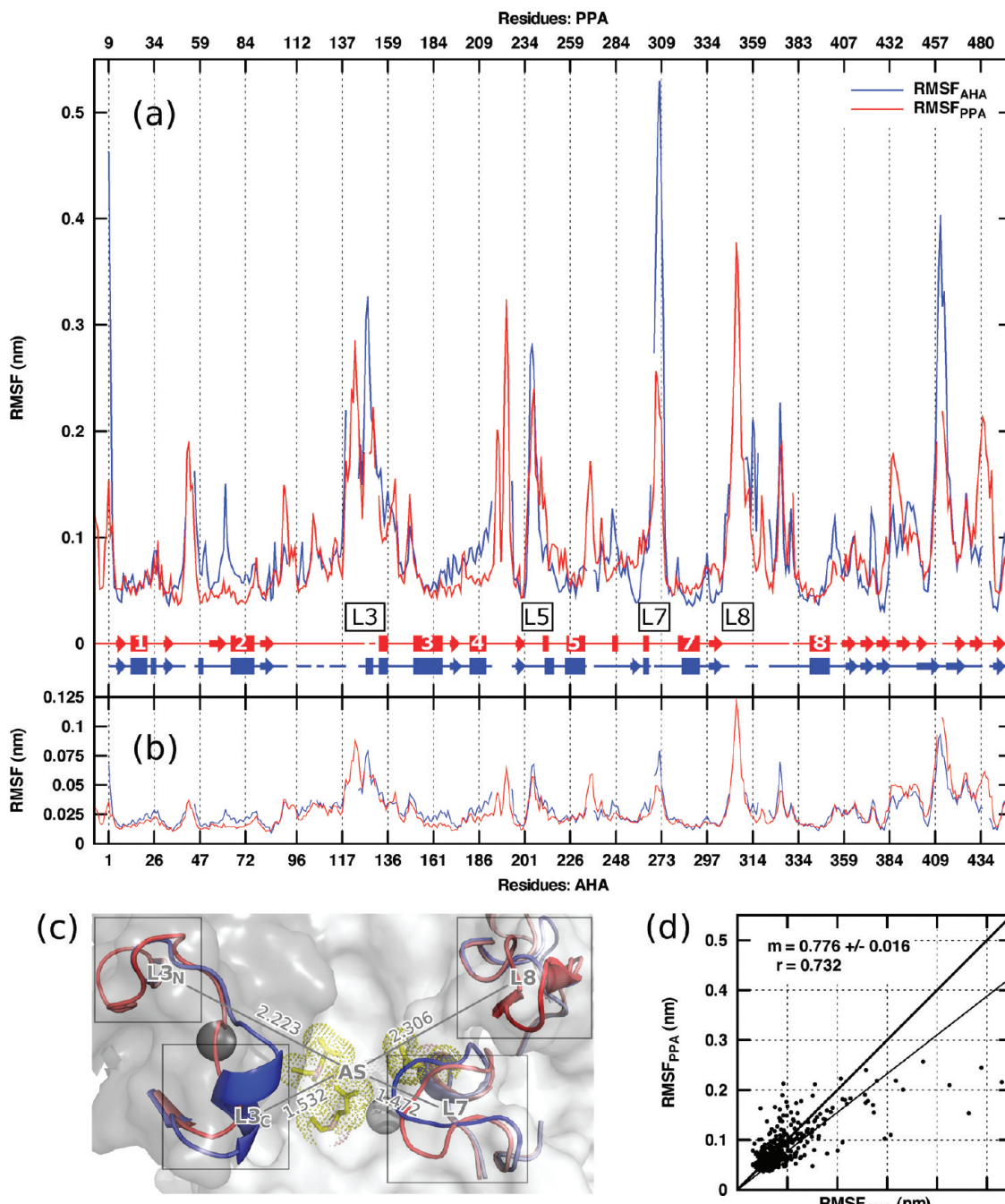


**Figure 4.** Aligned rmsf profiles as a function of alignment position computed on the metatrajectory (a) and on 100 ps intervals (b). The rmsf profiles of AHA (blue line) and PPA (red line) are shown as thick lines, broken in correspondence of gaps in the alignment; the four highly flexible loops mentioned in the text are outlined, and the most persistent secondary structures are represented schematically. (c) Close-up view of the two enzymes' substrate binding groove (represented as the transparent surface of PPA), where distances between the catalytic triad (AS, shown in yellow) and the most flexible regions in the surroundings are highlighted: **L3<sub>N</sub>** (PPA), **L3<sub>C</sub>** (AHA), **L7** (AHA), and **L8** (PPA). The backbone is colored as in Figure 1. Distances are ensemble averages computed between the centers of mass of the groups, and expressed in nanometers. (d) Correlation of flexibility of corresponding residues for AHA and PPA according to the structural alignment: the regression ( $m$ ) and correlation ( $r$ ) coefficients are displayed in the plot.

**L5** (203–206<sup>A</sup>, 236–239<sup>P</sup>) immediately follows the catalytic E200<sup>A</sup> (E233<sup>P</sup>) and features great conservation both in structure and in intensity of fluctuations (Figure 4). Significant differences between the two enzymes can be identified in the correlation of motions between **L5** and **L3**, greater in AHA as shown in Figure 5b, where relevant correlations between C<sub>α</sub> atoms of the two loops have been mapped on the structure of the two enzymes (see Methods). This marked divergence in the cor-

relation pattern may be connected with the absence, in AHA, of the C70–C115<sup>P</sup> disulfide bridge on the opposite side of domain B.

**L7** immediately follows a short helical structure carrying the third acidic catalytic residue (D264<sup>A</sup>, D300<sup>P</sup>). It is the most flexible region of the cold-active enzyme and features the greatest fluctuational differences between the two enzymes (Figure 4a). Dominant motions of **L7** involve oscillations to

**TABLE 2: Regions Featuring Relevant Differences in Flexibility between the Two  $\alpha$ -Amylases<sup>a</sup>**

AHA	PPA	domain	seq (AHA)	seq (PPA)	abbreviation
57–62	69–74	A	LQSRGG	LCTRSG	
92–95	<b>104–107</b>	B	AGSG	GSGA	
122–129	148–153	B	INNSDYGN	IE- -SYND	<b>L3<sub>C</sub></b>
268–274	305–311	A	HGGAG-N	HGAGGSS	<b>L7</b>
384–392	<b>432–440</b>	C	EDSTLTATV	DDWQLSSTL	
408–415	456–461	C	ELSADA K	DKV- -GNS	
432–437	<b>478–486</b>	C	NIGA- -WD	SISNSAQDP	
	52–55	A		TNPS	
	140–145	B		KCKTA	<b>L3<sub>N</sub></b>
	217–226	A		LNTNWFPAGS	
	269–271	A		WSG	
	347–354	A		NFVN GEDV	<b>L8</b>

<sup>a</sup> Bold intervals indicate which enzyme features higher fluctuations, while bold amino acid names highlight substitutions between the two enzymes; in the lower part of the table, the highly flexible insertions of PPA are listed.

and from the active-site groove, with amplitudes strongly enhanced in AHA (Figure 5a). Interestingly, in PPA, immediately above and in direct contact with **L7**, a highly flexible insertion is found (**L8**), which is the most flexible region of the mesophilic  $\alpha$ -amylase (Figure 4).

**L3** and **L7** are the two most mobile loops surrounding the active site, and in both cases, it is clear that highly flexible insertions in PPA (**L3<sub>N</sub>** and **L8**) are found in the immediate proximity of conserved regions (**L3<sub>C</sub>** and **L7**); we have shown that the latter regions are characterized by higher fluctuations in AHA, so that mobility of the substrate-binding site in PPA is shifted further away from the catalytic triad (Figure 4). The insertions in PPA appear to be of key importance in determining the overall flexibility of the mesophilic enzyme, as shown in Figure 4a, where gaps in the aligned sequence of AHA often correspond to peaks in the rmsf profile of the mesophilic  $\alpha$ -amylase. Furthermore, while the average flexibility of the two enzymes is comparable, if only matching residues are taken into account according to the structural alignment (i.e., insertions are ignored), the psychrophilic enzyme shows greater flexibility scattered throughout the entire protein, as shown in Figure 4d. Finally, analysis of the SAS of PPA shows that insertions exhibit on average more than double the SAS of PPA as a whole. Although a clear establishment of the role of the mesophilic enzyme longer loops and their flexibility in temperature adaptation is complicated by the evolutionary distance between the two organisms from which the two  $\alpha$ -amylases have been isolated,<sup>40,66</sup> taken together, these results suggest that dominant motions in PPA, when compared to its cold-active homologue, are displaced to few highly flexible, highly solvent accessible loop regions, and thus further away from the active site.

**Dynamic Properties of Loop 7.** The availability of crystallographic studies of both AHA and PPA in complex with oligosaccharidic substrate analogues (bound forms) has allowed us to analyze active-site motions in the free form in terms of its opening and closing, and to make some insightful considerations on its dynamics in solution as observed during our simulations. These studies<sup>61,64</sup> have shown that in both enzymes substrate binding causes significant displacements of **L7** toward the substrate, causing an apparent closure of the active-site groove.<sup>67,68</sup> Furthermore, a  $\sim$ 60° rotation of the side chain of D300<sup>P</sup> around the C<sub>α</sub>–C<sub>β</sub> dihedral ( $\chi_1$ ) is observed in PPA, possibly leading the catalytic aspartate to its catalytically active conformation. Conversely, in all available crystal structures of AHA, bound and free, the side chain of D264<sup>A</sup> is very similar to that found in the bound forms of PPA. Therefore, we have

focused our analysis on (i) the conformational fluctuations of **L7** and (ii) the rotation of the catalytic aspartate side chain around dihedral  $\chi_1$ .

The dynamics of **L7** in the free form have been analyzed using the first principal component ( $p_1$ ) of motion of the loop region (see Methods). In both enzymes, fluctuations along  $p_1$  identify an active-site opening/closing oscillation where positive values correspond to more open conformations; motions along  $p_1$  describe 67.2 and 40.1% of total variance for AHA and PPA, respectively. The extent of **L7** motions differs substantially between the two  $\alpha$ -amylases, as previously described (Figure 4), and the distribution of  $p_1$  values in the simulated ensemble (Figure 6a) shows that the high rmsf observed for **L7** in AHA arises from a multimodal distribution of sampled conformations, while in PPA **L7** motions are more restricted.

We have measured  $\chi_1$  dihedral values for all available crystal structures of the two enzymes, both in the presence (bound) or absence (free) of a substrate or inhibitor. Our measurements show that free structures of PPA exhibit  $\chi_1$  values around 60° (free<sub>PPA</sub>); all structures of AHA and bound structures of PPA, instead, feature  $\chi_1$  values around 150° (bound<sub>PPA</sub>; see also Supporting Information Text S3 and Figures S9 and S10). The distribution of  $\chi_1$  dihedral values in the simulated ensemble (Figure 6b) shows that, in both enzymes, conformations of the catalytic aspartic span three basins, two of which are in good agreement with crystallographic results and have been termed free<sub>PPA</sub> and bound<sub>PPA</sub>, in relation to values observed in crystal structures of PPA. The distribution also shows that in our simulations D264<sup>A</sup> possesses greater rotational freedom than that exhibited in available crystal structures, and even greater than D300<sup>P</sup>.

The joint distributions of  $p_1$  and  $\chi_1$  (Figure 6), instrumental in relating the behavior of **L7** and the catalytic aspartic-acid residue in the simulated ensembles, show that in AHA (Figure 6c, left) motions along  $p_1$  strongly correlate with specific D264<sup>A</sup> side-chain rotamers: values of  $\chi_1$  spanning the free<sub>PPA</sub> basin match positive values of  $p_1$ , while negative values of  $p_1$  correspond to the other two  $\chi_1$  basins, including the bound<sub>PPA</sub> basin. In order to assess if this behavior has converged in our simulations and it is not the consequence of the particular combination of *replicas*, we have repeated the analysis on a 28.6 ns metatrajectory composed of the four replicas featuring the most clear-cut convergence, both in terms of rmsd and of cosine content (see Supporting Information Figures S1 and S4). The results obtained (see Supporting Information Figure S8) are analogous to those shown in Figure 6c, and allow similar conclusions to those discussed here. These data suggest the presence of a strong interdependence between motions of **L7** and rotation of D264<sup>A</sup> around  $\chi_1$ , and in particular that more open conformations of the active site correlate with values of  $\chi_1$  corresponding to the free<sub>PPA</sub> basin; a similar correlated behavior cannot be identified for PPA (Figure 6c, right).

The observed dynamics of the active site of AHA suggest that the **L7** region, including catalytic D264<sup>A</sup>, undergoes conformational changes in the absence of substrate which may be related to the motions involved in reaching the transition state upon substrate binding. The same does not hold for PPA, and the low mobility of **L7** in the mesophilic enzyme is consistent with the computed high energy barrier between its free and bound microstates.<sup>68</sup> These marked differences in the extent and character of **L7** motions in AHA and PPA have prompted us to analyze the mechanistic determinants of this asymmetry. The structure and localization of **L7** in both enzymes suggests that it may be categorized as an  $\Omega$  loop, as

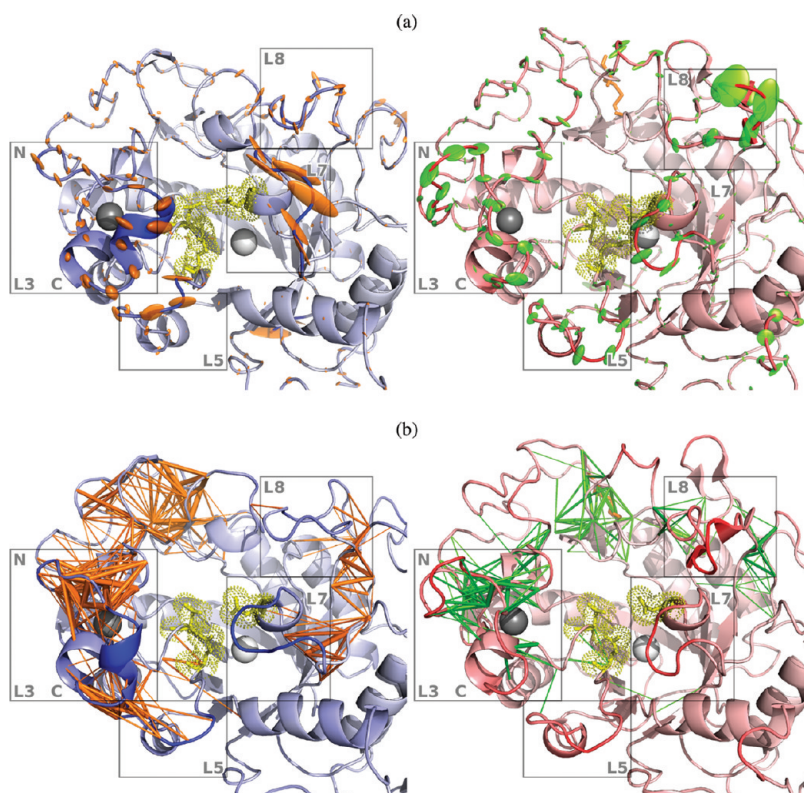


**Figure 5.** Computed anisotropic temperature factors for the *essential subspace* shown as ellipsoids for  $C_\alpha$  atoms, mapped on the average structure of the simulated ensembles (see Methods); correlation plots showing significant positive correlations between  $C_\alpha$  atoms of domains A and B (see Methods). The left and right panels picture AHA and PPA, respectively. The backbone is colored as in Figure 1.

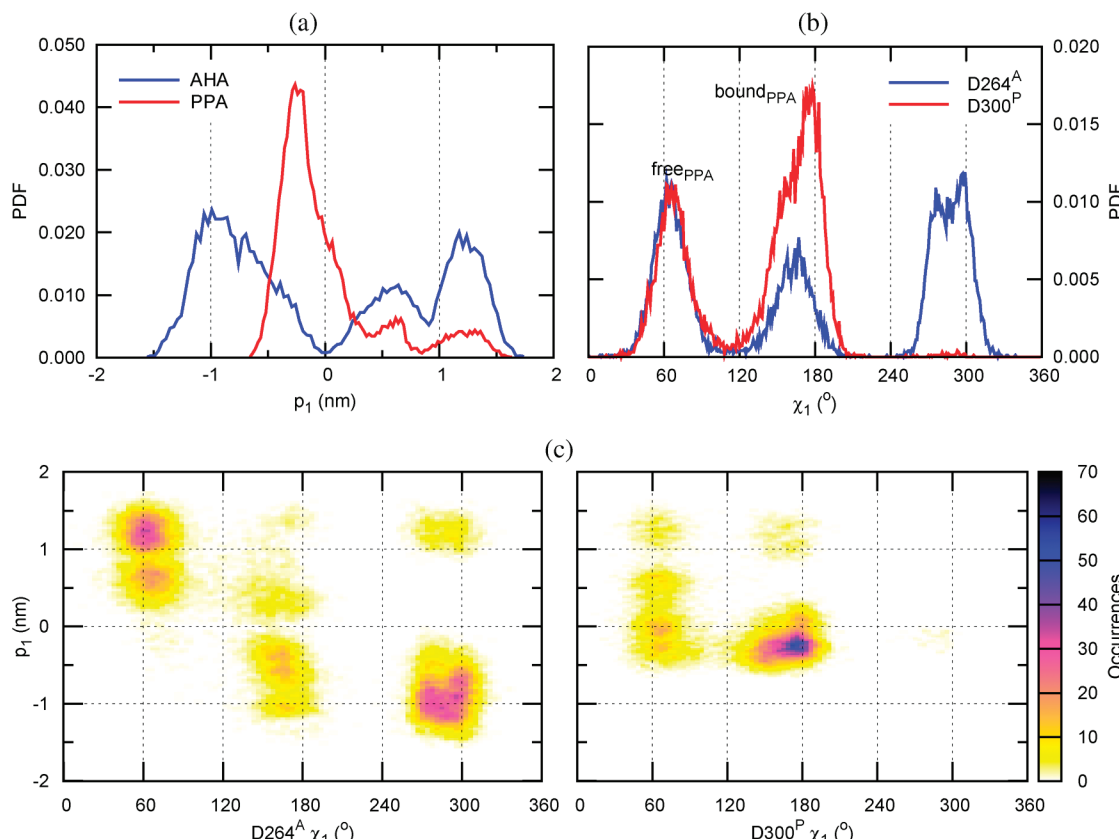


**Figure 6.** Distributions of (a) values of the first principal component of L7 motion and (b)  $\chi_1$  dihedral of D264<sup>A</sup>/D300<sup>P</sup> are joined (c) for AHA (left) and PPA (right); bin sizes have been set to one hundredth of the range of each data set.

shown for other  $\alpha$ -amylases.<sup>67</sup> The movement of these  $\Omega$  loops has been suggested to rely on backbone rotations of hinge

residues located at their extremities; we have thus proceeded to characterize the hinges of L7 movement in AHA and PPA,

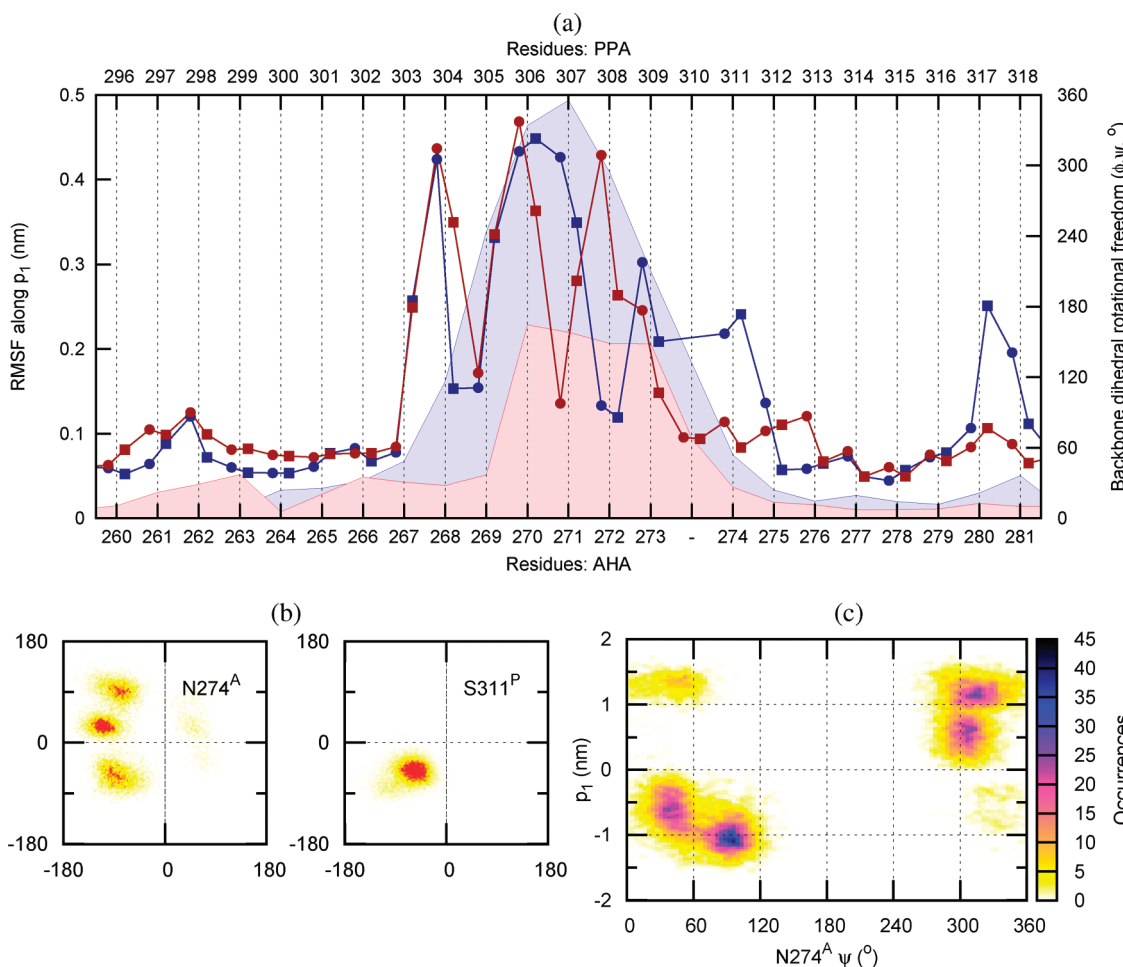


**Figure 7.** Profiles of dihedral rotational freedom (linespoints) of  $\phi$  (circles) and  $\psi$  (squares) for AHA (blue) and PPA (red) plotted with the rmsf along the first principal component of L7 motion  $p_1$  (shaded curves); Ramachandran plots of residues N274<sup>A</sup> (left) and S311<sup>P</sup> (right); joint distribution of N274<sup>A</sup>  $\psi$  values and motions along  $p_1$ ; bin sizes are the same as those used in Figure 6.

by measuring both  $C_\alpha$  fluctuations and backbone dihedral ( $\phi$  and  $\psi$ ) rotational freedom of L7 and its immediate surroundings.

Figure 7a shows both the  $C_\alpha$  rmsf along  $p_1$  and an estimation of the statistical dispersion of  $\phi$  and  $\psi$  values in the simulated ensemble (see Methods). The plot shows that  $C_\alpha$  flexibility profiles follow a bell-shaped curve, which is preceded by a few residues that feature marked rotational freedom, in particular R267<sup>A</sup>, G268<sup>A</sup>, and H269<sup>A</sup> (R303<sup>P</sup>, G304<sup>P</sup>, and H305<sup>P</sup>); these residues are well conserved in Cl<sup>-</sup>-dependent  $\alpha$ -amylases, and could work as the N-terminal hinges of L7 motion. Globally,  $\phi$  angles show good correspondence between the two  $\alpha$ -amylases, the most apparent differences involving  $\phi$  dihedrals of G271<sup>A</sup> and A272<sup>A</sup> (A307<sup>P</sup> and G308<sup>P</sup>), and probably due to the inversion of the position of an alanine and glycine residues in the two  $\alpha$ -amylase sequences. Greater differences are present in the  $\psi$  profiles, and particularly on the C-terminal side of the peak in the flexibility profiles, in correspondence with residue N274<sup>A</sup>, which features higher rotational freedom than S311<sup>P</sup>, as pointed out by the comparison of the two residues' Ramachandran plots (Figure 7b): while N274<sup>A</sup> interconverts between three distinct backbone conformations differing particularly for  $\psi$  values, S311<sup>P</sup> only adopts  $\phi$  and  $\psi$  values consistent with  $\alpha$ -helical conformations. Furthermore, the joint distribution of  $p_1$  and N274<sup>A</sup>  $\psi$  (Figure 7c) shows that the three backbone rotamers of N274<sup>A</sup>  $\psi$  correspond well with the peaks in the distribution of  $p_1$  values in AHA (see Figure 6a), suggesting that N274<sup>A</sup> could act as the C-terminal hinge of L7 motion,

and that its higher backbone rotational freedom could account for enhanced mobility of L7 in AHA.

## Conclusions

With the aim of contributing to the elucidation of the structural and dynamical features relevant for enzyme cold adaptation in the  $\alpha$ -amylase family, we adopt MD simulations to investigate and compare psychrophilic and mesophilic homologues: our extensive sampling of the two  $\alpha$ -amylases' phase space allows us to draw significant conclusions concerning the nanosecond-scale behavior of these enzymes at room temperature, and to precisely identify the regions where the most striking differences in the dynamic properties of these two enzymes are localized.

We find in both enzymes highly flexible regions, and the most noticeable differences in flexibility are located mainly in the surroundings of the substrate-binding groove and consist of the  $\beta$ - $\alpha$ -loops that protrude from the main domain's barrel structure. It has previously been reported that these loops are longer in the mesophilic enzyme, and thus feature regions which have no counterpart in the structural alignment of the two proteins (i.e., insertions) which extend further away from the core of the barrel, where the active site is located. Our findings show that the essential dynamics of PPA primarily involve these highly solvent accessible insertion regions, leaving the immediate surroundings of the active site, which feature greater

structural similarity between the two  $\alpha$ -amylases, comparatively more flexible in the psychrophilic enzyme. Increased active-site flexibility has often been considered as an adaptive trait in the context of temperature adaptation, and the likely interplay of other evolutionary phenomena related to the different nature of evolution in prokaryotes and eukaryotes<sup>40,66</sup> does not, in our opinion, necessarily rule out its possible relevance in this context.

Furthermore, previous crystallographic studies of the substrate-bound and free conformations of the two enzymes suggested the importance of key structural rearrangements in the binding and processing of small substrates.<sup>61,64</sup> In addition, it has been suggested for AHA that the kinetic parameters of substrate hydrolysis and the thermodynamic parameters of ligand binding are linked to improved molecular motions of the residues involved in substrate binding and catalysis.<sup>9</sup> Our detailed analysis of their active site has allowed us to identify concerted motions of a conserved highly flexible  $\Omega$  loop involved in substrate binding (**L7**) and a catalytic aspartic residue (D264<sup>A</sup>/D300<sup>P</sup>), whose rotation toward the catalytically competent conformation strongly correlates with loop closure in AHA. We were also able to identify the hinge residues of **L7** movement, where the most striking differences between the two enzymes are found, and in particular an asparagine (N274<sup>A</sup>) whose backbone dihedral rotation correlates with **L7** movement, and whose greater rotational freedom may account for the enhanced motions of **L7** in AHA. These results substantiate the presence of concerted and arguably functionally relevant motions in both enzymes even in the absence of substrate, suggesting that an interplay of motions intrinsic in the two enzymes may be important in performing their activity,<sup>69,70</sup> and that modulation of these dynamic properties could be significant in the context of their thermal adaptation.

**Acknowledgment.** We thank Prof. Richard Lavery for critical reading of the manuscript and Dr. Paolo Mereghetti and Dimitrios Spiliotopoulos for technical help and fruitful comments. This research was supported by the “Progetto Nazionale Ricerche in Antartide” and Cineca (Project-562 and Project-609).

**Supporting Information Available:** Details on the simulation setup and the equilibration procedure, supporting methods, and details on  $\chi_1$  measurements. This material is available free of charge via the Internet at <http://pubs.acs.org>.

## References and Notes

- (1) Smalås, A. O.; Leiros, H. K.; Os, V.; Willlassen, N. P. *Biotechnol. Annu. Rev.* **2000**, *6*, 1–57.
- (2) Russell, N. J. *Extremophiles* **2000**, *4*, 83–90.
- (3) Georlette, D.; Blaise, V.; Collins, T.; D’Amico, S.; Gratia, E.; Hoyoux, A.; Marx, J.-C.; Sonan, G.; Feller, G.; Gerday, C. *FEMS Microbiol. Rev.* **2004**, *28*, 25–42.
- (4) Siddiqui, K. S.; Cavicchioli, R. *Annu. Rev. Biochem.* **2006**, *75*, 403–433.
- (5) Antranikian, G.; Vorgias, C. E.; Bertoldo, C. *Adv. Biochem. Eng. Biotechnol.* **2005**, *96*, 219–262.
- (6) Hoyoux, A.; Blaise, V.; Collins, T.; D’Amico, S.; Gratia, E.; Huston, A. L.; Marx, J.-C.; Sonan, G.; Zeng, Y.; Feller, G.; Gerday, C. *J. Biosci. Bioeng.* **2004**, *98*, 317–330.
- (7) Gianese, G.; Bossa, F.; Pasarella, S. *Proteins* **2002**, *47*, 236–249.
- (8) Feller, G. *Cell. Mol. Life Sci.* **2003**, *60*, 648–662.
- (9) D’Amico, S.; Sohier, J. S.; Feller, G. *J. Mol. Biol.* **2006**, *358*, 1296–1304.
- (10) Wintrode, P. L.; Arnold, F. H. *Adv. Protein Chem.* **2000**, *55*, 161–225.
- (11) Fields, P. A.; Wahlstrand, B. D.; Somero, G. N. *Eur. J. Biochem.* **2001**, *268*, 4497–4505.
- (12) Russell, R. J.; Gerike, U.; Danson, M. J.; Hough, D. W.; Taylor, G. L. *Structure* **1998**, *6*, 351–361.
- (13) Lonhienne, T.; Gerday, C.; Feller, G. *Biochim. Biophys. Acta* **2000**, *1543*, 1–10.
- (14) Feller, G.; Lonhienne, T.; Deroanne, C.; Libioulle, C.; Beeumen, J. V.; Gerday, C. *J. Biol. Chem.* **1992**, *267*, 5217–5221.
- (15) Feller, G.; Payan, F.; Theys, F.; Qian, M.; Haser, R.; Gerday, C. *Eur. J. Biochem.* **1994**, *222*, 441–447.
- (16) Aghajari, N.; Feller, G.; Gerday, C.; Haser, R. *Protein Sci.* **1998**, *7*, 564–572.
- (17) Aghajari, N.; Feller, G.; Gerday, C.; Haser, R. *Structure* **1998**, *6*, 1503–1516.
- (18) Feller, G.; d’Amico, D.; Gerday, C. *Biochemistry* **1999**, *38*, 4613–4619.
- (19) D’Amico, S.; Gerday, C.; Feller, G. *J. Biol. Chem.* **2001**, *276*, 25791–25796.
- (20) D’Amico, S.; Gerday, C.; Feller, G. *J. Biol. Chem.* **2002**, *277*, 46110–46115.
- (21) D’Amico, S.; Marx, J.-C.; Gerday, C.; Feller, G. *J. Biol. Chem.* **2003**, *278*, 7891–7896.
- (22) D’Amico, S.; Gerday, C.; Feller, G. *J. Mol. Biol.* **2003**, *332*, 981–988.
- (23) Linden, A.; Wilmanns, M. *ChemBioChem* **2004**, *5*, 231–239.
- (24) Siddiqui, K. S.; Poljak, A.; Guilhaus, M.; Feller, G.; D’Amico, S.; Gerday, C.; Cavicchioli, R. *J. Bacteriol.* **2005**, *187*, 6206–6212.
- (25) Siddiqui, K. S.; Feller, G.; D’Amico, S.; Gerday, C.; Giaquinto, L.; Cavicchioli, R. *J. Bacteriol.* **2005**, *187*, 6197–6205.
- (26) D’Amico, S.; Collins, T.; Marx, J.-C.; Feller, G.; Gerday, C. *EMBO Rep.* **2006**, *7*, 385–389.
- (27) Siddiqui, K. S.; Poljak, A.; Guilhaus, M.; Francisci, D. D.; Curmi, P. M. G.; Feller, G.; D’Amico, S.; Gerday, C.; Uversky, V. N.; Cavicchioli, R. *Proteins* **2006**.
- (28) Aghajari, N.; Feller, G.; Gerday, C.; Haser, R. *Protein Sci.* **2002**, *11*, 1435–1441.
- (29) Papaleo, E.; Riccardi, L.; Villa, C.; Fantucci, P.; De Gioia, L. *Biochim. Biophys. Acta* **2006**, *1764*, 1397–1406.
- (30) Pandini, A.; Mauri, G.; Bordogna, A.; Bonati, L. *Protein Eng., Des. Sel.* **2007**, *20*, 285–299.
- (31) Olufsen, M.; Smalås, A. O.; Moe, E.; Brandsdal, B. O. *J. Biol. Chem.* **2005**, *280*, 18042–18048.
- (32) Rueda, M.; Ferrer-Costa, C.; Meyer, T.; Pérez, A.; Camps, J.; Hospital, A.; Gelpí, J. L.; Orozco, M. *Proc. Natl. Acad. Sci. U.S.A.* **2007**, *104*, 796–801.
- (33) Karplus, M.; McCammon, J. A. *Nat. Struct. Biol.* **2002**, *9*, 646–652.
- (34) Dodson, G.; Verma, C. S. *Cell. Mol. Life Sci.* **2006**, *63*, 207–219.
- (35) van Gunsteren, W. F.; et al. *Angew. Chem., Int. Ed. Engl.* **2006**, *45*, 4064–4092.
- (36) Papaleo, E.; Olufsen, M.; De Gioia, L.; Brandsdal, B. O. *J. Mol. Graphics Modell.* **2007**, *26*, 93–103.
- (37) Papaleo, E.; Pasi, M.; Riccardi, L.; Sambi, I.; Fantucci, P.; De Gioia, L. *FEBS Lett.* **2008**, *582*, 1008–1018.
- (38) Olufsen, M.; Brandsdal, B. O.; Smalås, A. O. *J. Mol. Graphics Modell.* **2007**, *26*, 124–134.
- (39) Olufsen, M.; Papaleo, E.; Smalås, A. O.; Brandsdal, B. O. *Proteins* **2007**, *71*, 1219–1230.
- (40) Spiwok, V.; Lipovová, P.; Skálová, T.; Dusková, J.; Dohnálek, J.; Hasek, J.; Russell, N. J.; Králová, B. *J. Mol. Model.* **2007**, *13*, 485–497.
- (41) Hess, B. *Phys. Rev. E* **2002**, *65*, 031910.
- (42) Caves, L. S.; Evanseck, J. D.; Karplus, M. *Protein Sci.* **1998**, *7*, 649–666.
- (43) van Buuren, A. R.; Marrink, S. J.; Berendsen, H. J. C. *J. Phys. Chem.* **1993**, *97*, 9206–9212.
- (44) Mark, A. E.; van Helden, S. P.; Smith, P. E.; Janssen, L. H. M.; van Gunsteren, W. F. *J. Am. Chem. Soc.* **1994**, *116*, 6293–6302.
- (45) van Gunsteren, W. F.; Berendsen, H. J. C. *Gromos-87 manual*; Biomos BV Nijenborgh 4, 9747 AG Groningen, The Netherlands, 1987.
- (46) Machius, M.; Vértesy, L.; Huber, R.; Wiegand, G. *J. Mol. Biol.* **1996**, *260*, 409–421.
- (47) Brayer, G. D.; Luo, Y.; Withers, S. G. *Protein Sci.* **1995**, *4*, 1730–1742.
- (48) Berendsen, H. J. C.; Postma, J. P. M.; Gunsteren, W. F. V.; Hermans, J. Intermolecular forces. In *Adv Appl Lipid Res*; Reidel: 1981; Vol. 331–332.
- (49) Hess, B.; Bekker, H.; Berendsen, H. J. C.; Fraaije, J. G. E. M. *J. Comput. Chem.* **1997**, *18*, 1463–1472.
- (50) Darden, T.; York, D.; Pedersen, L. J. *Chem. Phys.* **1993**, *98*, 10089–10092.
- (51) Kabsch, W.; Sander, C. *Biopolymers* **1983**, *22*, 2577–2637.
- (52) Jones, D. D. *J. Theor. Biol.* **1975**, *50*, 167–183.
- (53) Motono, C.; Gromiha, M. M.; Kumar, S. *Proteins* **2008**, *71*, 655–669.

- (54) Hubbard, S. J.; Thornton, J. M. *NACCESS* (computer program); Department of Biochemistry and Molecular Biology, University College: London, 1993.
- (55) Holm, L.; Sander, C. *Science* **1996**, *273*, 595–603.
- (56) Hünenberger, P. H.; Mark, A. E.; van Gunsteren, W. F. *J. Mol. Biol.* **1995**, *252*, 492–503.
- (57) Amadei, A.; Lissen, A. B. M.; Berendsen, H. J. C. *Proteins* **1993**, *17*, 412–425.
- (58) Papaleo, E.; Mereghetti, P.; Fantucci, P.; Grandori, R.; De Gioia, L. *J. Mol. Graphics Modell.* **2009**, *27*, 889–899.
- (59) Goldstein, R. A. *Protein Sci.* **2007**, *16*, 1887–1895.
- (60) Lipari, G.; Szabo, A. *J. Am. Chem. Soc.* **1982**, *104* (17), 4546–4559.
- (61) Qian, M.; Haser, R.; Buisson, G.; Duée, E.; Payan, F. *Biochemistry* **1994**, *33*, 6284–6294.
- (62) Qian, M.; Haser, R.; Payan, F. *Protein Sci.* **1995**, *4*, 747–755.
- (63) Ramasubbu, N.; Paloth, V.; Luo, Y.; Brayer, G. D.; Levine, M. J. *Acta Crystallogr., Sect. D* **1996**, *52*, 435–446.
- (64) Aghajari, N.; Roth, M.; Haser, R. *Biochemistry* **2002**, *41*, 4273–4280.
- (65) Ramasubbu, N.; Ragunath, C.; Mishra, P. J. *J. Mol. Biol.* **2003**, *325*, 1061–1076.
- (66) Rost, B. *Curr. Opin. Struct. Biol.* **2002**, *12*, 409–416.
- (67) André, G.; Tran, V. *Biopolymers* **2004**, *75*, 95–108.
- (68) Cheluvaraja, S.; Mihailescu, M.; Meirovitch, H. *J. Phys. Chem. B* **2008**, *112*, 9512–9522.
- (69) Radkiewicz, J. L.; Brooks, C. L. *J. Am. Chem. Soc.* **2000**, *122*, 225–231.
- (70) Rod, T. H.; Radkiewicz, J. L.; Brooks, C. L. *Proc. Natl. Acad. Sci. U.S.A.* **2003**, *100*, 6980–6985.

JP900790N